Journal of Hazardous Materials 189 (2011) 624–639

Contents lists available at ScienceDirect

Journal of Hazardous Materials

journal homepage: www.elsevier.com/locate/jhazmat

Sulfide oxidation and acid mine drainage formation within two active tailings impoundments in the Golden Quadrangle of the Apuseni Mountains, Romania

Mihaela Sima[a,*], Bernhard Dold[b,1], Linda Frei[c], Marin Senila[d], Dan Balteanu[a], Jűrg Zobrist[e]

[a] Romanian Academy, Institute of Geography, 12 Dimitrie Racovita St., Sector 2, Bucharest 023993, Romania
[b] Institute of Geochemistry and Mineralogy, University of Lausanne, Switzerland
[c] Swiss Federal Institute of Technology (EPFL), 1015 Lausanne, Switzerland
[d] Research Institute for Analytical Instrumentation, 67 Donath St., Cluj-Napoca 400293, Romania
[e] Swiss Federal Institute of Aquatic Sciences and Technology (Eawag), Ueberlandstr. 133, 8600 Dübendorf, Switzerland

ARTICLE INFO

Article history:
Received 24 August 2010
Received in revised form 10 January 2011
Accepted 17 January 2011
Available online 22 January 2011

Keywords:
Sulfide oxidation
Element mobility
Active tailings
Golden Quadrangle
Romania

ABSTRACT

Sulfidic mine tailings have to be classified as one of the major source of hazardous materials leading to water contamination. This study highlights the processes leading to sulfide oxidation and acid mine drainage (AMD) formation in the active stage of two tailings impoundments located in the southern part of the Apuseni Mountains, in Romania, a well-known region for its long-term gold-silver and metal mining activity. Sampling was undertaken when both impoundments were still in operation in order to assess their actual stage of oxidation and long-term behavior in terms of the potential for acid mine drainage generation. Both tailings have high potential for AMD formation (2.5 and 3.7 wt.% of pyrite equivalent, respectively) with lesser amount of carbonates (5.6 and 3.6 wt.% of calcite equivalent) as neutralization potential (ABA = −55.6 and −85.1 $tCaCO_3$/1000 t) and showed clear signs of sulfide oxidation yet during operation. Sequential extraction results indicate a stronger enrichment and mobility of elements in the oxidized tailings: Fe as Fe(III) oxy-hydroxides and oxides (transformation from sulfide minerals, leaching in oxidation zone), Ca mainly in water soluble and exchangeable form where gypsum and calcite are dissolved and higher mobility of Cu for Ribita and Pb for Mialu. Two processes leading to the formation of mine drainage at this stage could be highlighted (1) a neutral Fe(II) plume forming in the impoundment with ferrihydrite precipitation at its outcrop and (2) acid mine drainage seeping in the unsaturated zone of the active dam, leading to the formation of schwertmannite at its outcrop.

1. Introduction

The mining industry is one of the biggest waste producers in the world. In many cases, these often hazardous materials were stored randomly on the surface or underground, representing important sources of potential environmental contamination [1]. Sulfidic mine tailings are the major source for acid mine drainage (AMD) formation through sulfide oxidation in the metal mining industry. The geochemical and mineralogical investigations conducted so far and reported in many studies have focused on metalliferous tailings from both abandoned mining operations and those for which remediation measures have been implemented [2–13]. Liberation and retention processes of elements within tailings impoundments is a function of time (mainly during post-operation when a larger surface of tailings is exposed to oxidation) as well as of climate [14,15]. Only few studies have focused on the liberation and mobility of elements in active mine tailings [11,16]. If a tailings impoundment is properly managed, there should be no formation of AMD during operation, as oxidation should be slowed down by the complete water cover, which limits oxygen diffusion. However, often a lack of managing control or geotechnical construction features of the impoundments or climatic condition (e.g. arid climates), which do not allow the tailings to be maintained in completely saturated state, may promote sulfide oxidation during operation and the formation of AMD. In this study we present data from two active Romanian tailings impoundments that identify the geochemical processes that control AMD formation during operation of the tailings facility.

2. Regional setting

In Romania, the main mining-related concern is currently the long-term management of the waste deposits with a view

* Corresponding author at: Department of Physical Geography, Romanian Academy, Institute of Geography, 12 Dimitrie Racovita St., Sector 2, Bucharest 023993, Romania. Tel.: +40 213135990; fax: +40 213111242.
E-mail addresses: simamik@yahoo.com (M. Sima), bdold@ing.uchile.cl (B. Dold), lilipuce22@yahoo.fr (L. Frei), marinsen@yahoo.com (M. Senila), danbalteanu@clicknet.ro (D. Balteanu), zobrist@eawag.ch (J. Zobrist).
[1] Present address: Department of Geology, University of Chile, Plaza Ercilla 803, Santiago de Chile, Chile.

0304-3894/$ – see front matter © 2011 Elsevier B.V. All rights reserved.
doi:10.1016/j.jhazmat.2011.01.069

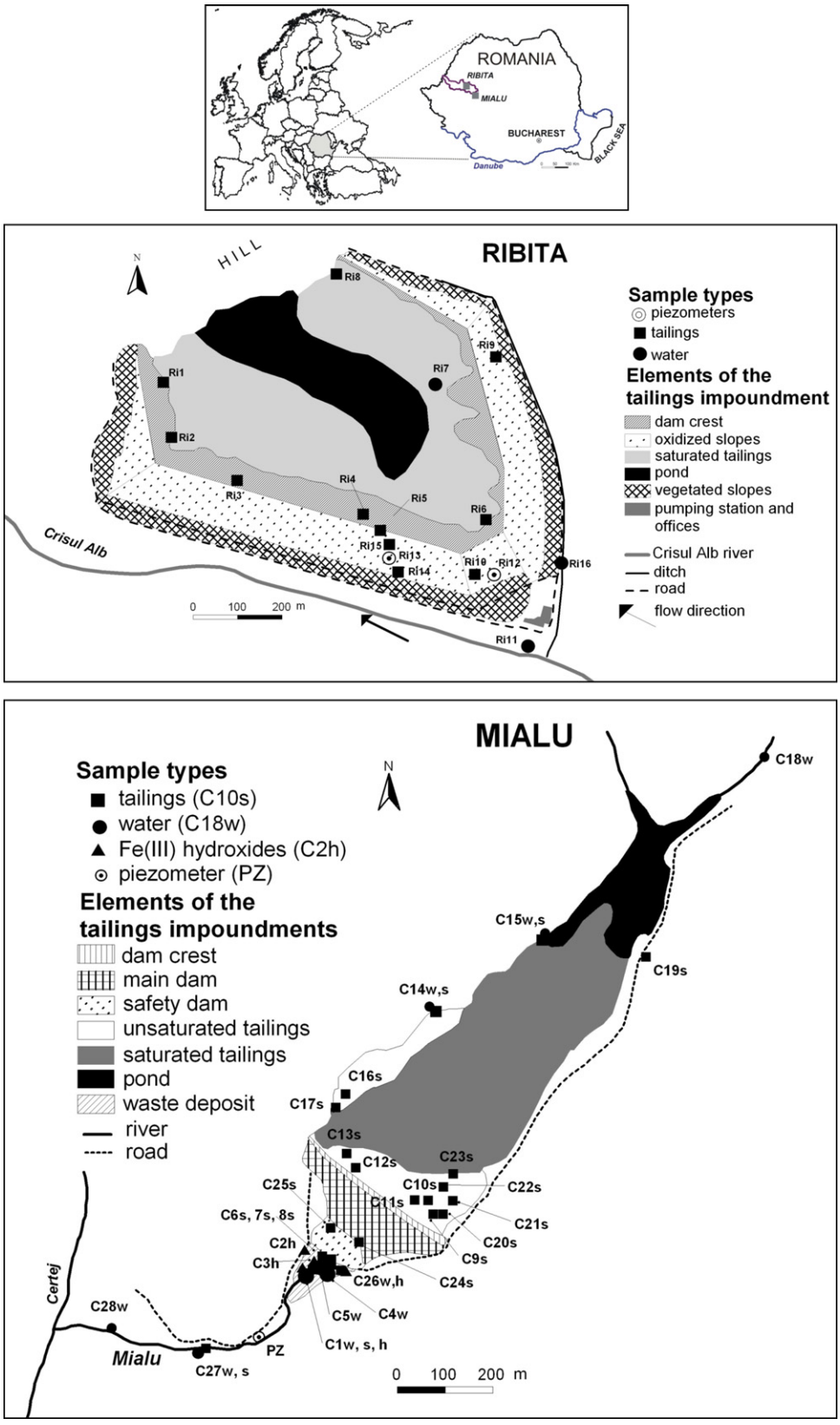

Fig. 1. Location of studied tailings impoundments (Ribita and Mialu) and sample sites.

to secure their physical and geochemical stability in order to reduce environmental pollution. Of principal concern is to minimize AMD formation and any associated environmental impact.

In the year 2000, two mine tailings dam failures in Maramures County, attracted international attention, notably due to the transboundary dispersal of metals and cyanide released during the events [17,18]. In view of this, issues such as mine waste depo-

sition and the use of dangerous substances were included in recent European directives (Seveso II or Toulouse I and the Mine Waste Directive) [19]. The severest mining accident in Romania occurred in the Certej River catchment in 1971, where a tailings dam, situated close to the Mialu tailings impoundment studied in this paper, failed resulting in over one-hundred deaths. Besides the human loss, the Certej River valley was inundated with 55,000 m^3 of mine tailings with significant implications for environmental quality and geomorphology [20].

The two studied tailings impoundments: *Ribita* (in the Crisul Alb river basin) and *Mialu* (in the Certej river basin) are located in the Metaliferi Mountains, the southern part of the Apuseni Mountains, and lie within the "Golden Quadrangle", a region well-known for its long history of metal mining activity (Fig. 1). Table 1 presents a summary of Ribita and Mialu tailings in terms of operation details, mineralogy and geochemistry (Table 1).

2.1. History and geographical setting

2.1.1. Ribita tailings impoundment

The *Ribita* tailings impoundment operated in the period 1986–2006, since the Valea Arsului porphyry-copper open pit has been exploited and is located partially in the Crisul Alb floodplain (at around 20–30 m distance from the present river channel; Fig. 1). The flood plains are characterized by mixed sequences of gravel and sandy layers of Lower Holocene age, representing a direct connection between tailings impoundment and aquifer. The tailings impoundment was built by a slope dam in steps, with an upstream filling, new parts of the embankment were built on top of the tailings deposited during the previous stage – the dam crest was therefore moving "upstream" (Fig. 2). The tailings impoundment stores 13.9 million m^3 of tailings and is 30 m in height.

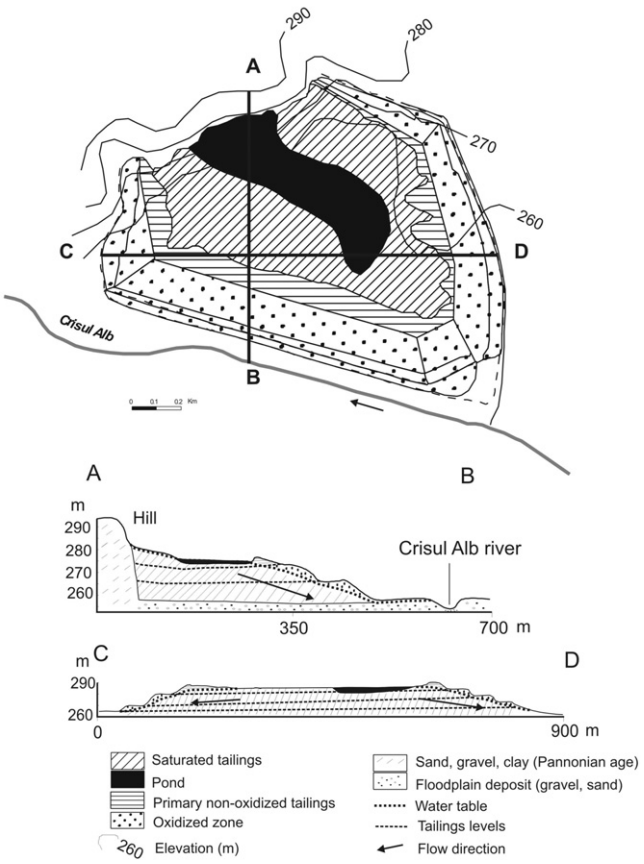

Fig. 2. Overview of Ribita impoundment.

2.1.2. Mialu tailings impoundment

The Mialu tailings impoundment was constructed in 1982–1984 in the Mialu river catchment, a left-side tributary of the main river, Certej and operated between 1984 and 2006. To build the impoundment, the valley was closed by a main dam made with waste-rocks from Coranda open pit (Fig. 3). The impoundment was then filled by an upstream system, in which the tailings were usually discharged from the top of the dam crest, creating a beach that became the foundation for subsequent extensions of the dam. The tailings dam stores 4.5 million m^3 of tailings and is 53 m in height. The impoundment is situated on the flood plain composed by mixed layers of Pleistocene gravels and sands.

3. Sampling and analytical methods

Sampling on the Ribita and Mialu tailings impoundments was undertaken in March 2006, during relatively cold weather conditions when both impoundments were still in operation. Surface and piezometer waters, tailings, soils, and iron hydroxide precipitates were collected from the Ribita and Mialu tailings impoundments in order to assess (1) their actual stage of oxidation and AMD formation and (2) their long-term behavior in terms of the potential for AMD generation. Main water sources (pond water or exit drainage pipe) have been sampled periodically after 6 months (August 2006),

Table 1
Main characteristics of Ribita and Mialu tailings impoundments.

Tailings impoundment	Ribita	Mialu
Operation time	1986–2006	1983–2006
Surface (ha)	60	43
Volume (m^3)	13,900,000	4,500,000
Deposition technique	Slope impoundment in steps with upstream filling	A main dam closing a river valley
Ore deposit type	a. Epithermal gold veins (Ruda-Barza, Bradisor, Musariu) b. Porphyry copper (Barza, Valea Morii)	a. Au–Ag–(Te) epithermal ore (Sacaramb) b. pollymetalic epithermal ore (Coranda-Hondol)
Ore mineralogy	a. Gold, silver, chalcopyrite, pyrite, sphalerite, galena, bornite, arsenopyrite, calcite and chlorite b. Chalcopyrite, magnetite, pyrite, bornite, sphalerite, tetrahedrite, galena, gold and molybdenite [21–23]	a. Gold–silver tellurides, rhodocrosite, alabandite, pyrite, pyrrhotite and chalcopyrite b. Galena, sphalerite, silver, gold, pyrite, chalcopyrite, tetrahedrite, bournonite and meneghinite [22,24]
Flotation circuit	pH > 8.5	pH > 8.5
Pyrite equivalent: average wt.% (min–max)	2.5 (0.6–8.6)	3.7 (1.4–6.5)
Calcite equivalent: average wt.% (min–max)	5.6 (0–17.2)	3.6 (0–7.1)
Acid-producing minerals	Pyrite, chalcopyrite	Pyrite, chalcopyrite
Neutralizing minerals	Calcite, dolomite	Calcite, dolomite
Average acid–base accounting (ABA) ($tCaCO_3$/1000 t)	−55.6	−85.1

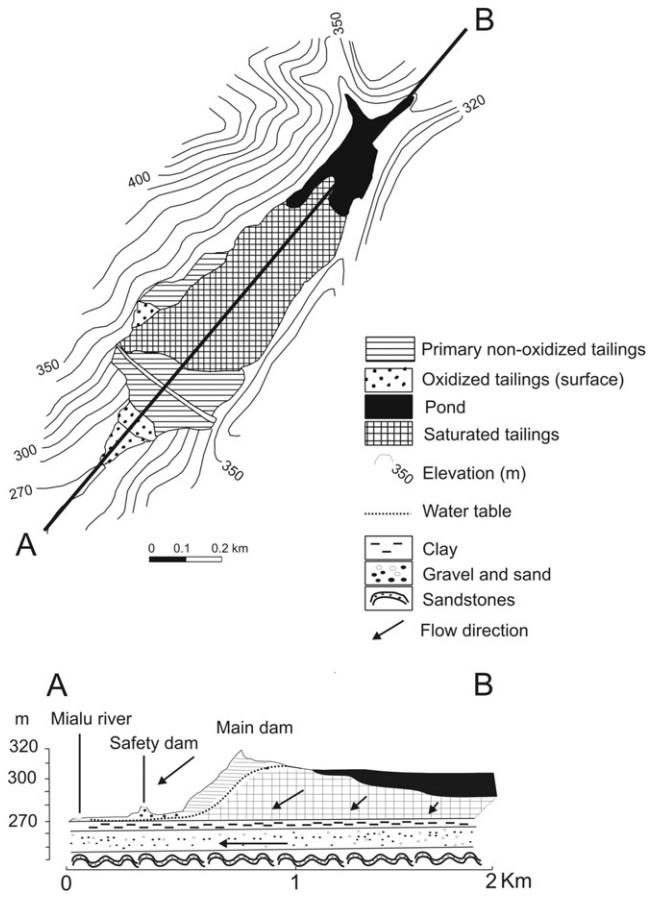

Fig. 3. Overview of Mialu impoundment.

1 and 3 years after ceasing the activity to investigate changes in metal mobility within the inactive impoundments.

3.1. Ribita tailings impoundment

A total of 19 solid and 5 water samples in the area of the Ribita tailings impoundment were collected. A detailed description of the samples is provided in Table 2, the sample positions are shown in Fig. 1 and the geochemical results in Appendix A.

Solid samples were collected from oxidation and primary zones, at the top of the dam as well as few profiles on the slopes of up to 70 cm depth in order to have a transect from the upper oxidation zone (0–25 cm depth) down to the primary zone, were oxidation has still not occurred. In the field, several parameters like sample depth, color, texture and paste-pH were measured (Appendices A and B). Samples were air dried directly after collection.

Water samples were filtered through 0.2 μm membranes with samples intended for cation analysis stabilized through the addition of suprapure HNO_3. Samples for both cation and anion analysis were maintained at 4 °C prior to analyse. Several parameters were measured on site: pH and Eh using a WTW pH 330i (corrected to SHE) and electric conductivity, dissolved O_2 and temperature (°C) with a WTW Multiline P4 instrument.

3.2. Mialu tailings impoundment

From the Mialu tailings impoundment a total of 46 samples were collected comprising solids and water samples and Fe(III) hydroxide precipitates (Table 2). Water evacuated from the dam through a pipe was sampled periodically, after 1 and 3 years of inactivity. The sampling and treatment procedure was the same as in case of the Ribita samples. The geochemical results are shown in Appendix B.

3.3. Analytical techniques

Around 100 g of each solid sample was milled between 30 s and 1 min, depending on the grain size, the final particle size being around 70 μm. Tailings samples were investigated by mineralogical and geochemical methods at the University of Lausanne: XRF (X-Ray Fluorescence) UniQuant 4, X-Ray diffraction (XRD) with a Philips instrument (Vertical goniometer PW1850, Conditions: 40 kV and 30 mA, Cu anode; CuKα1 radiation 1.5405 Å, Ni filter and monochrometer).

Sequential extractions were undertaken at Institute of Chemistry and Analytical Instrumentation Cluj, modified after Dold [25]. The reaction steps were as follows: 1 g sample was first extracted with 50 mL deionised water for 1 h to yield the water-soluble fraction (E1); then with 1 M ammonium-acetate, pH 4.5 for 2 h (exchangeable fraction, E2); afterwards with 0.2 M NH_4-oxalate, pH 3.0 in the dark for 1 h (ferric-oxyhydroxides fraction, E3) and finally with 0.2 M NH_4-oxalate, pH 3.0, heat in water bath 80 °C for 3 h (ferric-oxides fraction, E4).

Water samples were analysed by ICP-AES in Romania (SPECTROFLAME Germany) and by high resolution double focusing sector field ICP-MS at Eawag in Switzerland with Element2 (Thermo c/o Spectronex, Switzerland). Ion Chromatography (IC961 Methrom) was used to determine the main anions (F^-, Cl^-, NO_3^-, PO_4^{3-}, SO_4^{2-}). The accuracy and precision of metal analyses in water were assessed by a Certified Reference Material (NIST1643e, National Institute of Standards and Technology–NIST, Canada). Recovery degrees of the certified mean for 95% confidence interval were in the range of 96–106% for all analysed metals. Regarding anions analysis, a Certified Reference Material containing anions in wastewater (SPS-NU-WW1, LGC Promochem GmbH, Wesel, Germany) was used for quality control with recovery degrees ranging between 95 and 102% for all analysed anions. Calculation of element speciation and mineral saturation indices utilized the geochemical modeling code PHREEQC-2 [26] with the thermodynamic database from WATEQ4F [27].

Acid–base accounting (ABA) calculation was performed with the assumption that sulfur (S) is only in pyrite (FeS_2) and carbon (C) is only in calcite ($CaCO_3$). Neutral potential (NP) = wt.% $CaCO_3 \times 1000$ (tonnes $CaCO_3$ equivalent/1000 tonnes of tailings). Acid potential (AP) for the pH < 6.3 was calculated with the assumption that 1 mol of pyrite produces 4 mol of protons (H^+) that need 2 mol of calcite to be neutralized, based on the carbonate speciation in solution as a function of pH [28]. For pH ≥ 6.3 the calculation had in view that 1 mol of pyrite produces 4 mol of H^+ that need 4 mol of calcite to be neutralized.

4. Results and discussion

4.1. Ribita tailings impoundment

The deposition technique for tailings used at the Ribita impoundment differs to the Mialu impoundment, with additional dam steps being added above an original starter dam resulting in an upstream filling of the impoundment. As a result, there is an upward younging in the age of tailings material present within the dam (Fig. 2).

4.1.1. Stratigraphy, mineralogy and ABA

The stratigraphy of the *Ribita* tailings shows differences between material in the older part of the dam and the active upper part, where deposition was still ongoing during sampling. Tailings material in the lowest steps has been exposed to oxidation and

Table 2
Samples description in the Ribita and Mialu tailings impoundments (s: solid samples; w: water samples; h: iron hydroxides; A, B, C, D, E: different tailings layers).

Sample type	RIBITA (Ri)																							
Oxidized zone above primary one (lower oxidized steps) (depth in cm)							5 (surface)								92A (0–20) 92B (20–35)			10A (0–25)			14A (0–25)		
Primary non-oxidized tailings (depth in cm)	1A (0–20) 1B (20–50)		2 (70)	3 (surface)		4 (surface)			6 (58)		7 (50)		8 (50)		91 (70)			10B (25–50)			14B (25–50)		
Oxidized zone underlying primary one in lower oxidized steps (depth in cm)																					14C (30)		
Sediment from the ditch, bottom of the dam	16																							
Water samples	Impoundment lake 7			Drainage exit pipe 11					Piezometers water 12, 13									Ditch along the dam, at the bottom 16						
Sample type	MIALU (C)																							
Oxidized tailings (surface)		8s														17sA	17sB							
Primary non-oxidized tailings (surface)					10s	11s		12s		13s	14s	15s	16s					20s	21s	22s	23s	24s	25s	
Tailings in a oxidized profile from surface up to 60 cm (depth in cm)	6sA (0–10) 6sB (10–19) 6sC (19–29) 6sD (29–34) 6sE (34–44) 6sF (44–60)			9sA (0–8) 9sB (8–15) 9sC (15–19) 9sD (19–57) 9sE (57–70)																				
Fe(III) hydroxides	1h, 2h, 3h, 26h																							
Sediment from the ditch at the bottom of the dam	1s and 27s (Mialu river)																							
Soil	19s																							
Water samples	Impoundment lake 15w			Drainage exit pipe 1w		Piezometer water PZ				River Mialu 18w, 26w, 27w			Domestic well 28w					Small basins (at the dam foot) 4w, 5w					

weathering processes for around 20 years and a continuous low-pH (3.1–4) oxidation zone of 10–30 cm depth has formed. The underlying primary zone maintained neutral to alkaline pH (7–8.3). The active fresh tailings in the uppermost level showed a pH of around 8.3 and dominant grain size is sandy. The gangue mineralogy of the primary zone is represented by silicates (quartz, albite and muscovite), carbonates (calcite and dolomite), sulfides (pyrite, chalcopyrite, and sphalerite), and gypsum. The recent Ribita tailings (upper level) have an excess neutralizing potential (average 6.5 wt.% calcite and 1.4 wt.% pyrite), whereas the older levels have excess in acid potential (3.7 wt.% calcite and 5 wt.% pyrite). At the 2006 discharge point, fresh tailings mineralogy consists of quartz, alkali feldspar (mainly albite), calcite, micas (muscovite), chlorite, pyrite, chalcopyrite, gypsum and dolomite. The ABA for Ri2 (the fresh tailings) indicates a pyrite content of 0.6 and 4.9 wt.% calcite equivalent resulting in a positive sulfide net neutralization potential (NNP = +11 $tCaCO_3$/1000 t). However, in spite of the relatively low pyrite content in the older non-oxidized tailings (0.6–2 wt.%), the net neutralizing potential is negative (−33.8 $tCaCO_3$/1000 t). This could be mainly due to the low calcite content (5.6 wt.%) consumed in neutralizing reactions of the acidity coming from upper oxidized layer. The lowest levels of the impoundment are oxidized with an acid pH (2.6–4) showing orange-brown, yellowish and reddish precipitates in the oxidation zone. XRD data confirms the presence of secondary ferric mineralogy, such as jarosite and goethite and in certain samples no calcite could be detected. ABA for the oxidation zone indicates an elevated pyrite content (5.1 wt.%) and a low calcite (3.7 wt.%), resulting in a negative net neutralizing potential (−99.2 $tCaCO_3$/1000 t). The overall neutralizing potential for Ribita impoundment, with the assumption that all sulfide sulfur is associated with pyrite resulted in an average value of −55.6 $tCaCO_3$/1000 t.

4.1.2. Tailings geochemistry

The major elements in Ribita pond showed a relatively homogeneous distribution in the primary zone and a slight increase in the oxidation zone for most of them (Al, Si, Ti, Fe, S). The highest concentration in the primary samples was identified for those situated below the oxidation zone, as a result of migration from the upper oxidized zone during the wet season. Around 50–60% of the sample weight is represented by silicates (SiO_2), mainly quartz, but also albite, muscovite and chlorite. The heavy metals such as Cu and Zn show an enrichment in the primary samples situated below the oxidation zone, due to the mobilization of these metals from the acid oxidation zone. In contrast, Pb does not show this enrichment, possibly due to anglesite ($PbSO_4$) formation, which shows lower solubility than Cu and Zn sulfates. Magnesium (Mg) was slightly higher in the primary samples, probably related to silicates (chlorite, clinochlore) or dolomite identified by XRD; the same situation was identified for manganese (Mn) that could be present as carbonates (rhodochrosite) or as sulfates. Arsenic showed higher concentrations in the oxidation zone (250 mg/kg on average) compared to the primary zone (130 mg/kg) (Table 3).

Comparing the relative partition of the four fractions and the amount extracted in the sequential extractions, distinct differences arise between the oxidized solids (secondary material) in the top layer of the tailings (Ri10A) and the primary solids in the underlying layer of the profile (Ri10B). In the oxidized layer relative and absolute amounts of ferric-oxyhydroxides and -oxides are greater than in the primary zone (44,775 mg/kg compared to 15,208 mg/kg) (Fig. 4). This increase suggests a transformation from sulfide minerals to Fe(III) hydroxides and the relative leaching of some elements from the acid oxidation, resulting in a net increase of Fe in the oxidation zone. The amount of water soluble and exchangeable Fe is negligible in both layers. Mn displays an opposite extraction behavior than Fe. The relative and absolute amounts of fractions

Table 3
Mean, minimum and maximum concentration ± standard deviation (mg/kg) of relevant metals and As in the studied impoundments.

	Cu	Zn	Ni	Pb	Mo	As
Primary non-oxidized tailings Ribita, mean ± SD (min–max)	494 ± 55 (53–2620)	265 ± 93 (108–540)	–	236 ± 66 (62–1280)	12 ± 9 (6.7–17)	130 ± 59 (61–800)
Oxidized tailings Ribita, mean ± SD (min–max)	344 ± 65 (93–540)	163 ± 110 (108–249)	–	338 ± 70 (104–1280)	15 ± 9 (0–17)	250 ± 65 (61–800)
Primary non-oxidized tailings Mialu, mean ± SD (min–max)	60 ± 30 (0–184)	2000 ± 170 (121–3850)	20 ± 10 (0–248)	1000 ± 120 (45–8730)	–	300 ± 80 (0–630)
Oxidized tailings Mialu, mean ± SD (min–max)	150 ± 45 (0–248)	3160 ± 175 (510–5460)	3 ± 10 (0–17)	4400 ± 125 (322–6300)	2.6 ± 8 (0–13)	360 ± 85 (86–700)
Mialu surrounding soil	48	121	124	45	0	0

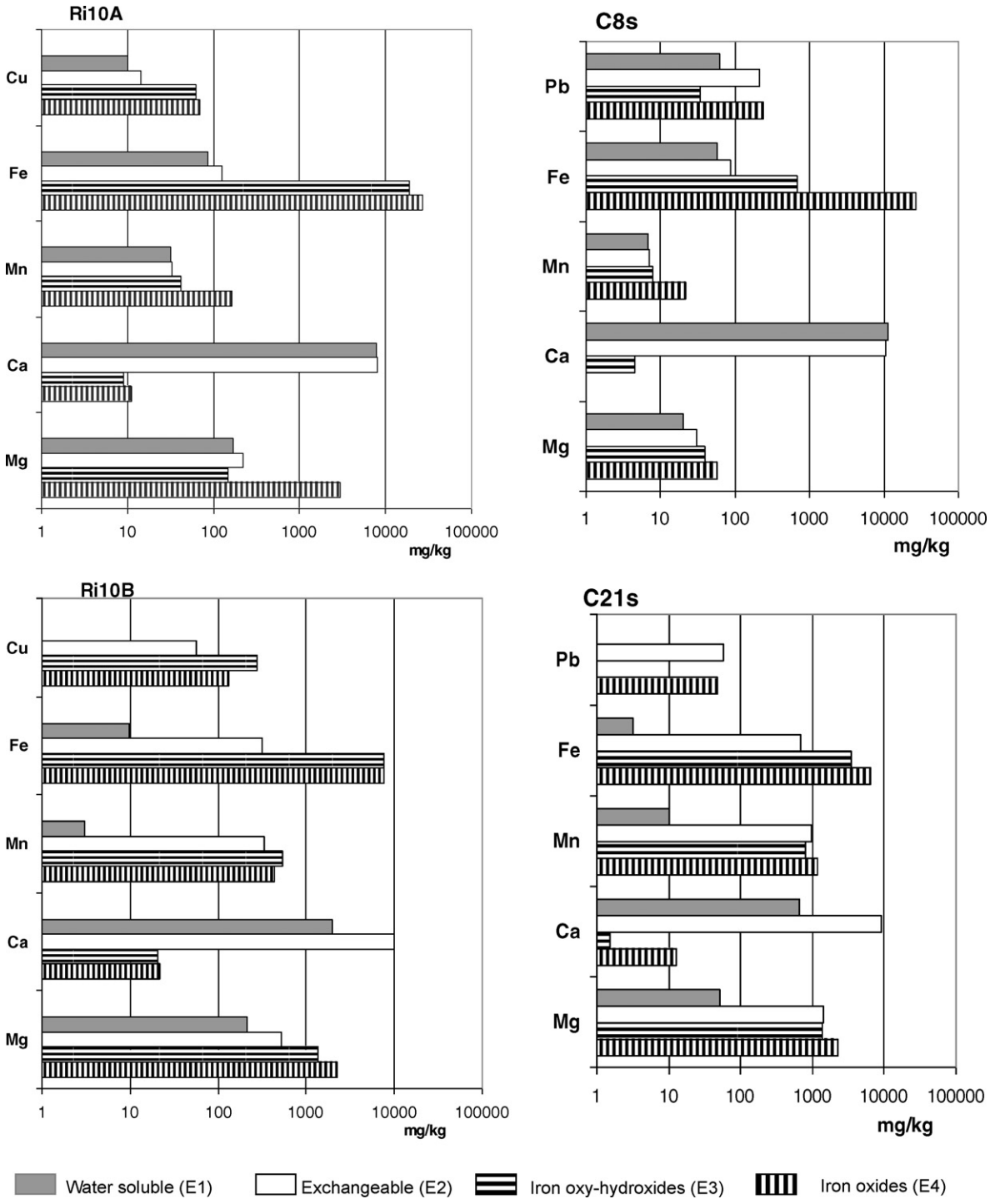

Fig. 4. Sequential extraction results for selected samples of the Ribita (Ri10A, Ri10B) and Mialu (C8, C21) impoundments.

E2 to E4 decrease in the oxidized layer. This observation can be explained by a washing out of soluble Mn(II) from the acidic and oxidized layer 10A. Indeed, the amount of exchangeable Mn in the layer underneath (Ri10B) is substantial and the total amount of Mn in the oxidized layer (33 mg/kg) is smaller than in the primary material (330 mg/kg). Furthermore, concentration of Mn in the water sampled in the piezometer of the tailings dam (Ri12 and Ri13) is high (2500 and 4000 μg/L, respectively). Cu exhibits a similar behavior as Mn, concerning the relative and absolute amount of extracted in and total metal content. Therefore, this suggests that Cu could also be leached out from the oxidation zone, similarly as reported in other tailings from porphyry copper systems [14]. The high amount of total Ca extracted in the first two extraction steps, E1 (7915 mg/kg) and E2 (7920 mg/kg), reveals that Ca is present as gypsum in the water soluble extract and as calcite in the exchangeable extract.

4.1.3. Aqueous geochemistry

Water samples were collected from the lake on top of the impoundment (Ri7), from the exit water pipe that flows to the main river (Crisul Alb) (Ri11), the 2 piezometers with water installed on the slopes (Ri12 and 13) and the channel that surrounds the

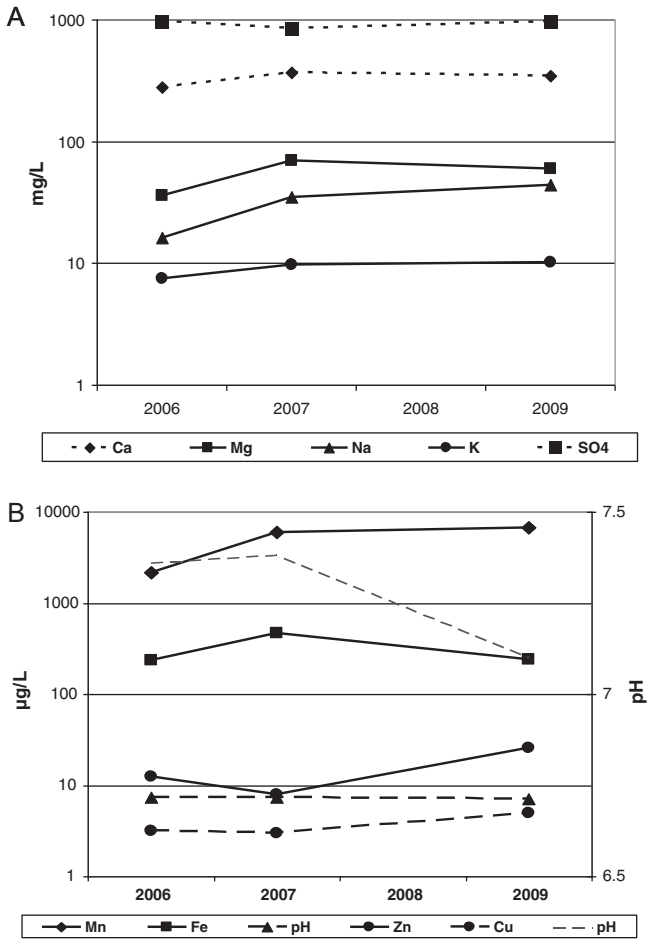

Fig. 5. Variation of major anions (A) and cations (B) in the Ribita outflow (Ri11).

impoundment (Ri16). The water pH range 6.9–7.7, the electrical conductivity is high for piezometers waters (2.5–2.7 mS/cm) and exit pipe water (1.2 mS/cm) and lower for top lake and channel water (Table 4). The redox potential (Eh) shows a similar trend to conductivity, higher in the piezometers water (up to 700 mV) and decreases to around 200 mV in the top lake waters.

Drainage in the Ribita tailings is still neutral, despite the visible oxidation in the older parts. However, some elements are mobile within the dam with highest concentrations in the piezometers (Ri12 and Ri13): 154 μg/L Zn, 6000 μg/L Fe, 4000 μg/L Mn, 50 μg/L Ni, 76 μg/L Cr and 114 μg/L As. Also in channels at different levels, the precipitation of Fe(III) hydroxides could be observed. The periodical measurements of water geochemistry reveal no significant changes in time, but a slight decrease in pH from 7.38 in 2007 to 7.1 in 2009. Several parameters show a slight increase especially from 2006 to 2007 (EC, Ca, Mg, Na, K, Cl, Mn, Fe, Ni, Co and As) (Fig. 5), suggesting to be the first signs of sulfide oxidation, subsequent neutralization and water–rock interactions in the tailings, but could also be the result of differences in the water budget in the impoundment.

4.2. Mialu tailings impoundment

Tailings grain size, the deposition technique, and history represent important factors in the potential generation of acid mine drainage during and post active operation of the impoundment. For the Mialu impoundment, the active discharge points with cyclones (spigots) are located on the dam crest and moved periodically along

Table 4
Hydrogeochemical data of major cations and anions in water samples, Ribita impoundment (data for metals are measured for dissolved fraction, DL: detection limit).

Sample code	pH	EC (ms/cm)	Ca (mg/L)	Mg (mg/L)	Na (mg/L)	K (mg/L)	SO_4 (mg/L)	Cl (mg/L)	NO_3 (mg/L)	Alk (meq)	Mn (μg/L)	Fe (μg/L)	Zn (μg/L)	Cu (μg/L)	Ni (μg/L)	Co (μg/L)	Cr (μg/L)	Pb (μg/L)	Cd (μg/L)	As (μg/L)
Ri7	7.65	0.4	52	5	2	3	156	1	0.2	0.6	1160	7	2	1.2	4	1	0.01	0.04	0.2	2
Ri11 March 2006	7.36	1.3	280	36	16	8	972	5	1	1.5	2170	238	13	3	22	7	0.5	3	0.4	10
Ri11 June 2007	7.38	1.9	369	70	35	10	850	10	0.5		5973	468	10	<DL	34	9	<1	<5	<1	18
Ri11 June 2009	7.1	1.8	345	60	44	10	977	10	<DL	1.4	6730	241	26	<5	16	<5	<5	<10	<5	7
Ri12	6.97	2.6	540	71	19	17	1388	5	1.7	5.1	2545	6092	30	1	2	3	0.1	0.1	0.1	110
Ri13	7.3	2.7	642	85	18	17	1608	5	0	3.3	4015	4260	154	3	50	4	76	3.5	0.1	114
Ri16	7.75		545	83	22	15	1540	4	0	2.8	929	213	32	2	0.3	1	0.5	0.2	0.05	4

Table 5
Mean values of several parameters analysed by XRF in primary non-oxidized tailings of Mialu and Ribita (SD: standard deviation).

Major elements	Mialu wt.% ± SD	Ribita wt.% ± SD	Trace elements	Mialu mg/kg	Ribita mg/kg
LOI	4.7	6.1	Zn	2000 ± 170	340 ± 93
SiO_2	66.1 ± 0.23	56.8 ± 0.25	Pb	1000 ± 120	160 ± 66
Al_2O_3	12.6 ± 0.17	16.5 ± 0.19	Ba	1000 ± 180	760 ± 120
Fe_2O_3	3.1 ± 0.09	5.1 ± 0.11	As	300 ± 80	130 ± 59
K_2O	5.3 ± 0.11	3.1 ± 0.09	Rb	200 ± 60	107 ± 51
S	2 ± 0.14	1.6 ± 0.15	Zr	200 ± 60	130 ± 47
CaO	3 ± 0.08	5.1 ± 0.12	Sr	130 ± 50	170 ± 60
MgO	1.4 ± 0.05	3.5 ± 0.09	V	90 ± 40	145 ± 47
MnO	0.32 ± 0.02	0.2 ± 0.023	Sb	70 ± 30	15 ± 12
TiO_2	0.55 ± 0.04	0.5 ± 0.037	Cu	60 ± 30	510 ± 55
P_2O_5	0.17 ± 0.02	0.24 ± 0.024	Cr	60 ± 30	27 ± 25
Cl	0.03 ± 0.008	0.04 ± 0.0093	Ce	40 ± 50	–
ABA	−85.09 ± 47	−55.64 ± 30	Co	40 ± 40	27 ± 9
–	–	–	Y	20 ± 10	20 ± 10
–	–	–	Ni	20 ± 10	–
–	–	–	Cd	20 ± 10	–
–	–	–	Ga	10 ± 6	16 ± 8
–	–	–	Mo	–	11 ± 9

it, in order to ensure a homogeneous distribution of tailings slurry. This method creates a hydraulic sorting of slurry with a different grain-size distribution: the coarser material (sand size) accumulates near the dam and spigot area thus raising the dam height, whilst the water with finer material are moved upstream into the tailings lake, where a more uniform grain-size distribution can be noticed. As a result of this grain-size sorting, the tailings deposited near the dam area have a higher sulfides content and permeability and lower water content, exposing this area to oxidation and weathering. Generally, fine horizons are poorer in sulfides than coarser layers because of gravity separation during deposition, so that lower sulfide contents are available for oxidation [11]. The higher content of Fe, S, Zn and Pb and lower of Ca, Mg was evidenced by XRF analysis of coarser samples (e.g. C7sA) compared to finer ones (C7sB).

4.2.1. Stratigraphy, mineralogy and ABA

Mialu mineralogy was characterized by the dominance of silicates (between 50 and 80 wt.%): quartz, K-feldspars and plagioclase, chlorite, illite and montmorillonite, muscovite. The sulfides identified in the tailings are pyrite, chalcopyrite and traces of molybdenite; carbonates (calcite and dolomite), sulfates (jarosite and gypsum) and iron oxides and hydroxides such as hematite and goethite. The total ABA for the Mialu tailings impoundment shows a pyrite content of 3.7 and 3.6 wt.% calcite equivalent, resulting in a negative sulfide net neutralization potential: −85.09 (t $CaCO_3$/1000 t), higher than of the Ribita impoundment.

The tailings impoundment stratigraphy at Mialu is similar to that of the Ribita impoundment. In terms of tailings deposition, the different construction techniques used for Mialu have resulted in the dam and fore-dam areas being exposed to oxidation (Fig. 3). Water seeping from the dam is acidic and results in the precipitation of Fe(III) hydroxides (Fig. 6). Thus, by the time when the impoundment was active several strongly oxidized zones situated below the main dam have been identified. The upper part of the impoundment was partly covered by water and partly formed on recent and fresh tailings with a neutral pH varying from 7 to 8.4. Below the safety dam a large greenish area (C8 s and C6 s samples in a depth profile) could be observed. These oxidized tailings with low paste-pH (3.2–4) present intercalated layers of different colors as a result of sulfide oxidation. As the observations were made in different seasons, variations in terms of humidity and the amount of water exiting the dam were noticed, indicating the importance of a seasonal cycle in AMD generation.

4.2.2. Tailings geochemistry

In the *Mialu* tailings impoundment pyrite was identified as the main sulfide in the primary tailings, with an average of 3.7 wt.% and a range of 1.4–6.5 wt.% (Table 1). In the majority of the primary tailings samples, calcite was present at a concentration of 3.6 wt.%. Calcite minerals induce a neutralization potential that will attenuate the effect of acidification sulfide oxidation. Zinc and lead were the main trace heavy metals found in the analysed tailings, with averages of 2000 mg/kg and 1000 mg/kg, respectively (Table 5). The sulfides were the primary sources of these metals: as sphalerite for Zn, with a calculated average of 0.3 wt.%, and galena for Pb, with an average of 0.11 wt.%. Galena and sphalerite oxidation normally occurs before pyrite oxidation and is responsible for producing circum-neutral mine drainage with Zn, Pb, SO_4^{2-} in solution. Arsenic was present in tailings at the average concentration of 300 mg/kg. Cu, Cd, Cr, Ni and Co were present at average concentrations of approximately 10–100 mg/kg and were mainly associated with sulfides. The geochemical data for all samples are given in Appendix B.

In comparison with other primary tailings samples, the sample C13s (dark-grey in color), taken at the top of the dam, had the highest concentrations of Pb (8.7 g/kg), high S (3.45 wt.%), Fe (4.96 wt.%), Zn (3.8 g/kg), Cu (184 mg/kg), Ni (24 mg/kg), and Ag. This provides further evidence of higher sulfide content within coarser tailings material.

The sample C15s, taken in the shallow waters of the pond and with the presence of Fe(III) hydroxide had the highest Al concentration (10.8 wt.%) and Fe concentration (3.06 wt.%). The high Fe concentration may reflect the presence of iron hydroxides. Samples taken from an oxidized profile of around 50 cm depth (C6s with A, B, C, D, E and F being different layers differentiated by color) contained more Fe, S, Co, Zn, Pb and Cu than the mean content of the primary samples. As this sample site was located at the foot of the small dam, an enrichment of elements transported by mine drainage from the top to the basement might explain this.

Near the C6s profile, a greenish surface sample was collected (C8s), with pH 3.4, characterized by high content of S (6.5 wt.%), K (5.9 wt.%), Fe (4.4 wt.%), Ca (3.5 wt.%), Pb (0.7 wt.%), and presence of Ag (0.005 wt.%). In comparison with C6s, Zn was very low (0.05 wt.%). Jarosite [$KFe_3(SO_4)_2(OH)_6$] was identified by XRD in this sample. The colored tailings taken at the ancient discharge point (C17sA and C17sB) were different in terms of color and paste-pH: blue-green with pH 3.6 (C17sA) and grey-brown with pH 4.4 (C17sB) (Appendix B). XRF results show that C17sA had 2.61 wt.% of

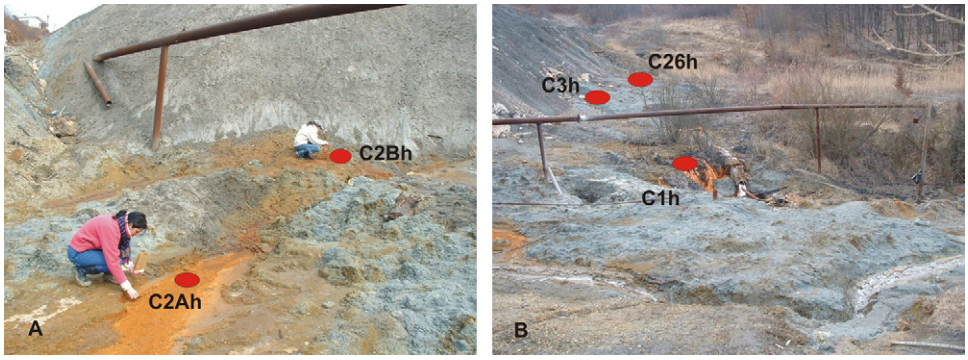

Fig. 6. The location of Fe(III) hydroxides samples (Mialu impoundment).

S and C17sB 1.58 wt.% of S. This can be correlated with the presence of jarosite in XRD pattern of C17sA.

Sequential extraction was undertaken for two samples from the primary (C21s) and oxidized (C8s) tailings (Fig. 4). It can be noticed high amounts of Fe(III) oxy-hydroxides and oxides (27,510 mg/kg) in the C8 sample as a result of transformation from sulfide minerals, data consistent with the XRD results indicating the presence of secondary products such as jarositeand goethite. The high content of Ca in the E1 and E2 extraction steps (11,450 mg/kg and 10,715 mg/kg respectively) reveals that Ca is present as gypsum in the water soluble extract and as calcite and dolomite in the exchangeable one. As for bivalent cations, a stronger enrichment of Pb in the oxidized sample in the exchangeable fraction (240 mg/kg) was identified, possibly present as secondary anglesite, reflecting the high mobility of this metal at low pH (around 4). Mg and Mn show a similar pattern as Ca in the primary non-oxidized sample (C21s), with higher concentrations in the exchangeable and iron oxides fraction. High Ca, Mg and Mn in the exchangeable fraction indicates that gangue carbonates are at least partly Mg- and Mn-bearing calcites, typical for hydrothermal Fe oxide Cu–Au systems [7]. Mg and Mn primary peaks in iron oxides and oxy-hydroxides fractions (3650 and 2000 mg/kg respectively) may be related to the dissolution of secondary hydroxides and oxides.

4.2.3. *Aqueous geochemistry*

The drainage of the Mialu tailings impoundment (C1w), collected by an internal drainage system (Fig. 6B), was characterized by a neutral pH (6.9) and high concentrations of dissolved metals (1074 μg/L Zn, 3693 μg/L Fe, 6680 μg/L Mn and 30 μg/L Ni). Sulfide oxidation was occurring in the active impoundment. This process was the earliest stage, where neutralizing minerals could maintain a neutral pH. Relatively high concentrations of SO_4^{2-} and Fe are typical for drainage water of oxidizing sulfide minerals such as pyrite. Sphalerite [ZnS] present in the Mialu impoundment primary tailings is identified as the source of Zn found in

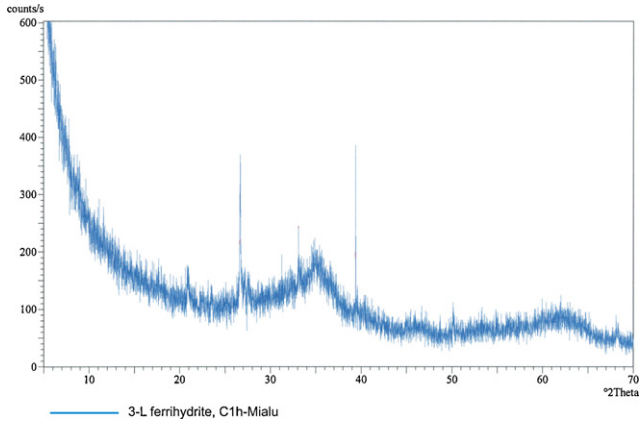

Fig. 7. XRD patterns for Fe(III) hydroxides samples C1h (Mialu impoundment).

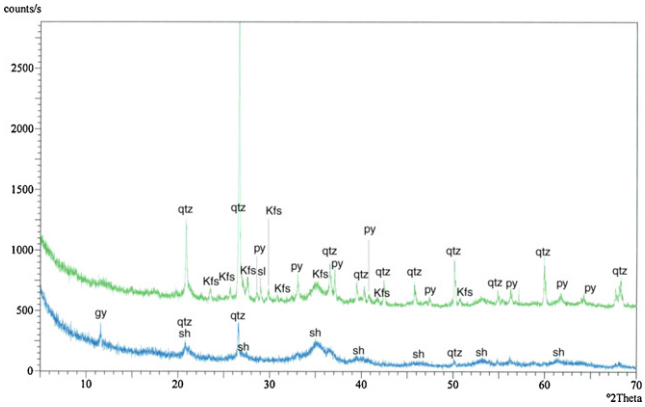

Fig. 8. XRD patterns for Fe(III) hydroxides sample C2Bh (Mialu impoundment) before (lower) and after (upper) acid leaching (abbreviations: qtz: quartz; kfs: K-feldspar; pz: pyrite; sl: sphalerite; gy: gypsum; sh: schwertmannite).

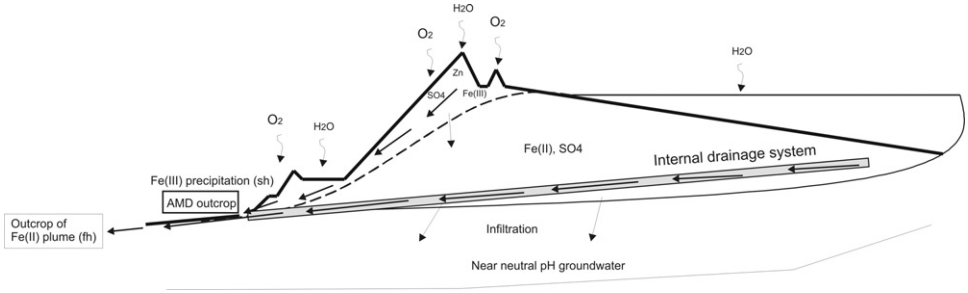

Fig. 9. Schematic model of iron mobilization AMD formation at Mialu impoundment.

Table 6
Hydrogeochemical data of major cations and anions in water samples, Mialu impoundment (data for metals are measured for dissolved fraction, DL: detection limit).

Sample code	pH	Eh (mV)	EC (mS/cm)	Ca (mg/L)	Mg (mg/L)	Na (mg/L)	K (mg/L)	SO_4 (mg/L)	Cl (mg/L)	NO_3 (mg/L)	Mn (μg/L)	Fe (μg/L)	Zn (μg/L)	Cu (μg/L)	Ni (μg/L)	Co (μg/L)	Cr (μg/L)	Pb (μg/L)	Cd (μg/L)	As (μg/L)
C1w (July 2005)	6.6							1900	66	3.7	17,000	16,000	3490					28	4.9	
C1w (March 2006)	6.9	347	1.9	191	31.6	12	9.3	536	24.7	1.1	6680	3690	1074	1.4	30	11	0.2	0.25	3.7	18
C1w (August 2006)	7.1			573	67	54	68	1520	2.6	0.1	15,000	20,000	517	1.8	121	12	1.2	1.2	0.9	
C1w (September 2006)	6.7			314	45	24	23	933	39	1	2200	4400	545	3.7	21	6.2	3.4	1.8	0.7	76
C1w (July 2007)	6.5			418	63	39	48	1180	37	2	6600	32,300	1140	4	56	22.4	3.3	<5	16	298
C1w (June 2009)	6.6			500	73.5	56.4	89.8	1609	69.1	0.5	–	34,200	4270	11	68	26	<5	4	16	156
C4w	2.9	709	–	488	194	10.7	10.3	3985	11.3	1.7	1500	20,430	186,200	7213	1600	457	141	201	923	99
C5w	6.96	503	4.2	24	4.9	5.3	<1	54	3.5	7.2	37	32	78	12	2.32	0.15	0.03	0.52	0.24	–
C15w	6.9	275	1.1	53	9.7	8.3	3.8	214	13.9	0.4	7018	2207	142	0.96	13	20	0.26	0.35	0.53	2.3
C18w	7.1		0.4	49	24.3	4.1	1.1	130	1.9	0.1	1.6	14	<DL	0,7	0.16	0.07	0.3	0	<DL	2.3
C26w	6.7	381	2.53	506	46	19.3	11.3	1905	23.5	0.1	7,740	34,360	15,880	7	265	102	<DL	0	18.3	7.1
C27w	6.95		1.8	321	43.8	20.4	19.5	897	38.2	0.8	9997	9034	3366	9.13	58	22	0.2	0.6	12	62
C28w	6.96	481	1.2	119	24.3	45.3	46.8	164	87.4	51	88	49	69	3	1.6	0.5	0.2	0	0.12	2.3
PZ (piezometer downsteam)	7.1		0.7	120	37	17	13	78	4	39	2	5880	60	9	25	22	10	84	5	27

solution (1074 μg/L in C1w, 15,880 μg/L in C26w and 3366 μg/L in C27w). As the ore was a "polymetallic deposit", other metals, notably Cu, Co, Cd, Pb, Ni and metalloid As, are also present in water (Table 6), but in lower concentrations reflecting their lower abundance in the deposit and their relative low solubility under circum-neutral pH. It is relevant to highlight that high Ca concentrations reflect the buffering of acid produced by calcium carbonate present in the impoundment. Water seeping from the dam through the drainage pipe (C1w sample) was sampled periodically in different seasons (results are presented in Table 6). It is important to note the variations in metal composition during different seasons with a higher concentration of elements during the summer and a higher dilution in the spring or autumn.

At the foot of the tailings dam several outcrops of AMD with the precipitation of secondary Fe(III) hydroxides could be observed (samples C1h, C2h, C3h and C26h). Two different ways of Fe(III) hydroxides formation can be highlighted. At the outflow of the drainage pipe (C1w, C1h), which collects seepage water in the center bottom of the impoundment (Fig. 6B), the pH is neutral and the Fe(III) hydroxide precipitating is a 3-line ferrihydrite (Fig. 7). This suggest that iron is transported as Fe(II) at reducing conditions through the saturated part of the tailings impoundment, this is supported by geochemical equilibrium modeling with PHREEQC. When it outcrops at the drainage tube to the oxidizing conditions, the Fe(II) auto-oxidizes fast to Fe(III) due to the neutral pH conditions, which results in the less crystalline 3-line ferrihydrite, sign of fast hydrolysis [29]. In contrast, only some meters uphill from the C1 pipe outcrop, the groundwater level in the dam seeped and formed outcrops with AMD and the precipitation of schwertmannite (C2h; Figs. 6A and 8). The presence of schwertmannite suggest that the transport of Fe (possibly as Fe(III)) was under acid condition as a effect of sulfide oxidation in the unsaturated areas of the dam. This was observed in a similar setting in another active impoundment in Chile [7].

5. Conclusions

The Ribita and Mialu tailings impoundment have high potential for AMD formation and show clear signs of sulfide oxidation and AMD formation although they were still in operation.

The Ribita tailings impoundment was in operation for more than 20 years, so that the tailings deposited at the lower slope oxidized and a low pH-oxidation (3.1–4.1) zone up to 30 cm was formed, characterized by the precipitation of Fe(III) hydroxides. The liberation of metal cations such as Zn, Ni, Mn or oxyanions such as As is visible in the piezometer and pipe waters even at relatively high pH (6.7–7) through sulfide oxidation processes. With advanced oxidation and precipitation of Fe(III) hydroxides enough acidity is produced to install low-pH conditions at the tailings surface, forming the conditions necessary to mobilize bivalent metal cations such as Cu, Ni, and Zn. The negative average net neutralization potential indicates that the total neutralization potential would not be sufficient in the future to prevent acid generation by sulfide oxidation.

At Mialu impoundment early stage oxidation of sphalerite, galena and pyrite had already started in the impoundment. Due to the deposition technique used at Mialu, the dam area has a coarser grain size and also higher sulfide concentration and is unsaturated. These characteristics lead to sulfide oxidation yet during operation with the liberation of Fe(III) in the unsaturated oxidation zone. The visual results of these processes are:

(1) A neutral Fe(II) plume which outcrops at the pipe and is characterized by the formation of 3-line ferrihydrite. The source of

this Fe(II) plume can be (a) sulfide oxidation with the liberation of Fe(III) in the oxidation zone and subsequent microbiological reduction at the oxidation front [30] and (b) iron from the surrounding soils.

(2) An outcrop of AMD is present at the foot of the dam where schwertmannite is formed. The presence of schwertmannite indicates that the flow of these solutions is acid. The origin of the acidity is seen in the sulfide oxidation taking place in the unsaturated coarser material of the dam. This leads to the acid Fe(III)-rich solutions, percolating towards the foot of the dam, were schwertmannite precipitates (Fig. 9).

In order to prevent the observed AMD formation in active mine tailings, following measures could reduce this risk: the use of non-reactive material for the dam construction, compactation of the dam material in order to limit water and oxygen flow and increase stability and complete water saturation of the impoundment in order to prevent oxidation in the beach area. As the tailings impoundments are located in a humid climate (700–800 mm/year rainfall and 500–600 mm/year evaporation) a possible measure to prevent sulfide oxidation could include the maintenance of the impoundment in a water saturated state by flooding. However, this must include important measures for dam stabilization.

Acknowledgements

The funding by the Swiss-Romanian Cooperation Program on 'Environmental Science and Technology in Romania—ESTROM', JRP Grant No. IZ6120-107015 (2005–2008) is greatly acknowledged. The authors are grateful to Dr. Graham Bird for his helpful comments and English corrections. We thank the reviewers for their comments who greatly improved the manuscript.

Appendix A. XRF data for Ribita solid samples.

	Non-oxidized tailings								Oxidized tailings									
	Ri1A	Ri1B	Ri2	Ri3	Ri4	Ri6	Ri7	Ri8	Ri10B	Ri14B	Ri15	Ri91	Ri5	Ri92A	Ri92B	Ri10A	Ri14A	Ri14C
pH	7.3	7	8	8.1	8.25	7.1	7.6	7.5	7.8	6.25	8.85	7.7	3.6	4.1	3.3	3.1	3.4	3.1
Depth (cm)	0–20	20–50	70	Surface	Surface	58	50	50	25–50	25–50	30	70	Surface	0–20	20–35	0–25	0–25	30
Texture	Sand	Sand	Sand	Sand	Sand	Sand	Sand	Sand	Sand	Sand	Sand	Sand	Sand	Sand	Sand	Sand	Sand	Sand
Color	Grey	Grey-light brown	Grey	Grey	White grey	Grey	Grey	Grey	Grey	Grey	Grey	Grey	Orange	Red	Yellow-white	Red-orange	Grey	Yellow, green
wt.%																		
LOI	7.57	5.27	5.14	5.66	8.7	4.83	6.1	5.96	6.11	6.73	5.42	5.96	9.2	6.36	5.82	6.45	6.25	16.06
SiO_2	54.63	58.21	59.05	55.22	55.07	60.2	58.03	56.48	56.62	54.86	56.81	56.5	48.86	53.42	58	53.25	54.04	42.42
Al_2O_3	16.64	16.16	16.76	16.71	15.68	16.25	16.26	16.33	17	16.1	16.59	17	14.45	15.85	16.31	15.56	16.31	10.56
Fe_2O_3	4.98	4.81	4.35	4.11	6.76	4.02	4.41	5.21	5.2	5.74	5.42	6.38	9.17	8.46	5.63	8.89	8.86	12.67
K_2O	3	3.36	3.17	3.13	2.74	3.31	3.03	3.1	3.17	2.97	3.31	3.12	3.27	3.06	3	3.39	3.33	2.45
S	1.84	1.87	0.617	2.01	1.99	1.36	1.64	1.76	1.17	2.26	1.4	1.45	5.49	3.23	3.4	3.83	3.3	8.64
CaO	5.85	5.1	5.38	7.43	3.85	4.82	5.27	5.72	4.63	5.09	4.86	3.1	4.91	3.68	2.84	3.12	2.88	4.17
MgO	3.51	3.19	3.48	3.56	3.48	3.23	3.27	3.26	3.77	3.64	3.74	3.72	2.78	3.54	2.75	3.18	2.77	0.71
MnO	0.204	0.208	0.198	0.222	0.157	0.191	0.183	0.22	0.225	0.332	0.224	0.183	0.129	0.124	0.055	0.1	0.106	0.0183
TiO_2	0.54	0.559	0.548	0.632	0.451	0.516	0.507	0.568	0.522	0.521	0.508	0.539	0.517	0.594	0.536	0.596	0.575	0.799
P_2O_5	0.237	0.234	0.265	0.311	0.207	0.208	0.225	0.262	0.229	0.243	0.223	0.225	0.252	0.329	0.199	0.282	0.322	0.022
Cl	0.0346	0.042	0.0062	0.052	0.0051	0.044	0.0389	0.048	0.0123	0.05	0.073	0.069	0.0112	0.057	0.0208	0.0198	0.0168	n.d.
ppm																		
As	183	169	118	61	203	118	121	165	87	141	98	112	800	145	61	216	202	72
Ba	630	960	780	480	377	690	640	960	690	950	990	980	940	1060	820	1240	1120	3560
Co	19	15	n.d.	21	55	24	8.6	22	19	46	30	42	97	49	107	143	163	93
Cr	50	22	10	29	43	20	26	47	11	23	12	34	29	43	n.d.	23	24	27
Cu	153	94	81	53	81	93	88	132	660	1330	750	2620	93	351	433	322	326	540
Ga	16	18	15	21	n.d.	14	16	15	13	16	14	13	19	12	13	13	16	12
Pb	185	112	119	62	610	105	132	192	97	137	75	117	149	104	118	182	197	1280
Sr	173	156	193	184	103	168	200	190	167	158	174	155	154	186	176	183	165	193
V	160	136	160	157	118	126	146	151	166	141	133	160	124	181	162	169	189	129
Y	20	14	18	28	13	20	18	21	20	22	17	17	14	14	19	9.4	10	n.d.
Zn	427	276	275	149	349	261	316	410	408	540	281	379	249	108	127	190	188	114
Zr	117	174	131	164	81	127	122	177	107	133	127	113	134	144	136	144	150	352

Appendix B. XRF data for Mialu solid samples.

Samples	pH	Depth (cm)	Texture	Color	LOI (wt.%)	SiO_2 (wt.%)	Al_2O_3 (wt.%)	Fe_2O_3 (wt.%)	K_2O (wt.%)	S (wt.%)	CaO (wt.%)	MgO (wt.%)	MnO (wt.%)	TiO_2 (wt.%)	P_2O_5 (wt.%)	Cl (wt.%)
C1s	–	River channel	–	Grey	7.10	60.61	11.14	6.21	4.63	3.85	2.87	1.200	0.252	0.4	0.181	0.0560
C6sA	3.2	0–10	Sand	Orange	9.24	57.81	8.30	8.48	4.59	5.98	2.47	0.528	0.200	0.386	0.131	0.0279
C6sB	5.52	10–19	Sand	Grey	7.80	60.88	10.62	5.45	6.46	4.13	2.04	0.552	0.081	0.439	0.105	0
C6sC	6.17	19–29	Sand	Dark-grey	8.58	57.00	10.71	6.13	5.30	4.72	3.39	1.600	0.303	0.406	0.142	0.0350
C6sD	3.8	29–34	Sand	Red	10.54	52.32	9.03	9.00	5.14	6.84	3.15	1.430	0.345	0.359	0.177	0.0255
C6sE	4	34–44	Clay	White	10.35	53.12	10.27	6.61	6.08	6.28	3.96	0.957	0.177	0.463	0.116	0.0258
C6sF	6.1	44–60	Sand	Grey	6.96	61.20	13.26	5.25	6.35	2.42	1.53	0.973	0.294	0.521	0.145	0
C7sA	6.3	River channel	Coarse Sand	Dark-grey	5.84	60.50	14.37	3.40	9.66	2.72	1.24	0.505	0.046	0.623	0.146	0.0264
C7sB	6.3	River channel	Sand	Grey	4.29	68.64	13.02	2.62	4.66	0.778	2.92	1.530	0.344	0.484	0.207	0.0072
C8s	3.4	Surface	Sand	Grey-blue-green	9.50	53.51	9.76	6.29	7.20	6.52	4.88	0.437	0.023	0.477	0.057	0.0213
C9sA	8.35	0–8	Sand	Light grey	3.65	69.06	12.96	2.16	4.53	1.71	2.86	1.340	0.272	0.788	0.191	0.0301
C9sB	7.87	8–15	Sand	Dark grey	4.35	66.03	13.07	3.10	5.02	2.19	3.03	1.510	0.366	0.536	0.179	0.0430
C9sC	7.9	15–19	Sand-clay	Dark brown	4.68	62.26	13.00	3.45	4.79	2.03	5.91	1.940	0.594	0.542	0.220	0.0334
C9sD	7.88	19–57	Sand	Brown	4.24	68.08	10.94	3.03	4.98	2.24	3.41	1.470	0.302	0.431	0.150	0.0610
C9sE	7.6	57–70	Sand	Dark grey	5.61	63.03	12.01	4.36	7.22	2.02	2.4	1.310	0.426	0.441	0.161	0.0056
C10s	8.12	Surface	Sand	Pink	4.08	65.50	17.23	2.38	5.44	0.85	1.6	1.410	0.196	0.619	0.203	0.0216
C11s	7.9	27	Sand	Pink-grey	2.77	73.80	11.34	1.67	4.62	1.57	1.79	1.030	0.141	0.599	0.153	0.0395
C12s	8.14	24	Coarse sand	Light grey	3.29	76.61	10.04	2.38	3.43	1.09	1.09	0.931	0.129	0.374	0.119	0.0089
C13s	8.16	Surface	Sand	Dark grey	9.16	55.71	11.34	7.09	6.92	3.45	2.36	1.250	0.456	0.382	0.117	0.0022
C14s	7.45	River channel	Sand	Light grey	5.55	60.33	17.21	3.61	4.91	0.729	3.73	1.830	0.717	0.556	0.249	0
C15s	7	River channel	Sand	Red, grey	6.58	54.81	20.40	4.38	6.25	1.74	2.33	1.840	0.305	0.483	0.229	0.0510
C16s	7.22	20	Sand	Grey	3.50	74.76	9.09	2.68	3.24	2.12	2.11	1.110	0.175	0.376	0.127	0.0430
C17sA	3.6	Surface	Sand	Grey-green	4.36	68.25	11.69	4.47	6.46	2.61	0.647	0.505	0	0.473	0.073	0.0246
C17sB	4.42	Surface	Sand	Grey-brown	3.89	68.04	12.01	4.68	6.88	1.58	1.23	0.424	0.049	0.457	0.155	0.0071
C19s	8.05	Dam' slope	Clay	Intense red soil	6.61	57.09	19.85	9.57	3.16	0.033	0.831	1.570	0.125	0.774	0.134	0.0104
C20s	7	15	Sand	Grey	4.41	68.92	12.22	2.67	4.69	1.15	2.64	1.480	0.275	0.562	0.195	0.0064
C21s	7.8	15	Sand	Grey	3.79	67.92	12.96	2.11	4.53	2.22	3.44	1.450	0.248	0.604	0.183	0.0640
C22s	7.72	15	Sand	Grey	4.19	65.58	13.17	2.33	4.96	2.98	3.69	1.320	0.251	0.72	0.186	0.0570
C23s	8.1	15	Sand-clay	Pink-grey	5.26	60.37	15.21	3.09	5.48	2.83	3.68	2.020	0.271	0.944	0.202	0.0430
C24s	7.65	25	Sand	Grey-brown	5.06	62.53	12.45	3.13	6.19	2.42	4.56	1.640	0.473	0.491	0.200	0.0590
C25s	7.54	20	Sand	Dark grey	4.69	66.47	12.16	3.04	6.36	1.5	2.84	1.360	0.350	0.448	0.151	0
C27s	6.95	River channel	Sand	Grey	4.13	66.07	12.62	2.67	4.87	2.32	3.91	1.670	0.313	0.616	0.195	0.0490

Samples	Zn (mg/kg)	Pb (mg/kg)	Ba (mg/kg)	As (mg/kg)	Rb (mg/kg)	Zr (mg/kg)	Sr (mg/kg)	Cu (mg/kg)	Sb (mg/kg)	Co (mg/kg)	V (mg/kg)	Cr (mg/kg)	Y (mg/kg)	Ni (mg/kg)	Ga (mg/kg)	Ag (mg/kg)	Mo (mg/kg)	Cd (mg/kg)	Ce (mg/kg)
C1s	3890	4860	2200	540	137	167	130	166	119	44	49	49	13	0	11	14	0	0	0
C6sA	5120	6300	2570	580	124	180	115	181	147	265	42	41	10	10	0	16	0	0	0
C6sB	2840	6220	1880	323	184	175	118	151	197	46	55	38	10	0	10	23	0	0	0
C6sC	5460	6040	1310	376	143	143	101	230	124	37	63	46	17	8	0	0	13	20	0
C6sD	4870	5340	1260	700	146	147	113	248	122	465	58	34	8.7	17	0	0	0	16	11
C6sE	3460	6030	2300	454	203	199	155	204	160	199	65	60	13	0	10	35	0	0	46
C6sF	4140	1860	1700	298	177	197	109	150	85	36	97	62	19	0	0	0	11	20	0
C7sA	2250	1360	2650	156	276	206	191	51	171	171	87	63	19	0	19	0	0	0	0
C7sB	920	428	1420	381	157	150	150	38	59	33	82	45	16	0	11	0	0	0	0
C8s	510	7140	2810	86	271	228	176	104	150	84	64	41	0	0	9	49	0	0	0
C9sA	1000	265	1080	301	156	222	101	45	43	31	120	94	21	0	11	0	0	0	0
C9sB	1990	281	1090	336	175	160	126	50	53	28	97	51	20	24	13	0	0	0	22
C9sC	1400	460	1210	392	159	222	183	61	64	29	95	94	16	11	13	0	0	0	0
C9sD	1570	880	1410	361	152	172	122	66	59	57	65	46	16	0	9	0	0	0	103
C9sE	3080	1500	2690	167	194	178	123	75	15	36	64	30	13	17	16	13	0	0	0
C10s	790	382	1380	307	210	184	150	56	75	14	146	142	26	17	19	0	0	0	0
C11s	950	284	1480	211	141	191	107	41	64	21	84	107	17	0	8	0	0	0	0
C12s	1750	227	730	314	99	148	58	41	57	62	46	49	13	10	0	0	0	0	0
C13s	3850	8730	1440	423	162	134	93	184	95	35	48	23	13	24	13	19	0	24	47
C14s	930	550	1540	620	214	172	203	133	102	0	125	96	24	0	20	0	0	0	21
C15s	1070	730	1320	630	299	171	142	131	133	0	182	171	30	0	27	0	0	0	26
C16s	1820	420	1520	495	98	124	89	52	89	59	71	69	13	0	0	0	0	0	0
C17sA	580	351	1560	183	174	199	101	0	48	0	89	0	9.4	0	0	13	0	0	0
C17sB	1450	322	1790	226	198	177	140	79	41	42	81	43	14	0	11	0	0	0	0
C19s	121	45	450	0	171	194	298	48	0	46	188	161	34	124	26	0	0	0	0
C20s	3630	202	1210	348	149	149	122	23	54	29	83	29	20	0	11	0	0	11	0
C21s	1300	227	1160	252	156	199	124	22	51	0	91	44	20	0	11	0	0	0	0
C22s	1580	297	1310	317	181	225	112	26	71	0	92	43	24	0	14	0	0	0	0
C23s	1420	377	1380	507	206	192	126	58	95	18	199	140	34	15	15	0	0	0	0
C24s	3070	450	1550	285	196	202	157	81	45	28	69	97	18	0	10	0	0	0	0
C25s	1750	720	1370	216	185	175	117	54	43	28	58	53	16	0	12	18	0	28	0
C27s	1060	399	1620	447	164	204	150	44	63	0	122	15	24	0	13	0	0	0	0

References

[1] F.G. Bell, L.J. Donnelly, Mining and its Impact on the Environment, Taylor & Francis Group, London, 2006.
[2] H. Holmström, B. Öhlander, Oxygen penetration and subsequent reactions in flooded sulphidic mine tailings: a study at Stekenjokk, northern Sweden, Appl. Geochem. 14 (6) (1998) 747–759.
[3] T. Al, D. Blowes, C. Martin, L. Cabri, J. Jambor, Aqueous geochemistry and analysis of pyrite surfaces in sulfide-rich mine tailings, Geochim. Cosmochim. Acta 61 (1998) 2353–2366.
[4] H. Holmström, U. Salmon, E. Carlsson, P. Petrov, B. Öhlander, Geochemical investigations of sulfide-bearing tailings at Kristineberg, northern Sweden, a few years after remediation, Sci. Total Environ. 273 (1–3) (2001) 111–133.
[5] J. Ljungberg, B. Öhlander, The geochemical dynamics of oxidising mine tailings at Laver, northern Sweden, J. Geochem. Explor. 74 (1–3) (2001) 57–72.
[6] B. Műller, M. Axelsson, B. Öhlander, Adsorption of trace elements on pyrite surfaces in sulfidic mine tailings from Kristineberg (Sweden) a few years after remediation, Sci. Total Environ. 298 (2002) 1–16.
[7] B. Dold, L. Fontbote, A mineralogical and geochemical study of element mobility in sulfide mine tailings of Fe oxide Cu–Au deposits from the Punta del Cobre belt, northern Chile, Chem. Geol. 189 (3–4) (2002) 135–163.
[8] B. Dold, Element flows associated with marine shore mine tailings deposits, Environ. Sci. Technol. 39 (40) (2006) 752–758.
[9] B. Dold, J.E. Spangenberg, Sulfur speciation and stable isotope trends of water-soluble sulfates in mine tailings profiles, Environ. Sci. Technol. 39 (15) (2005) 5650–5656.
[10] B. Öhlander, B. Müller, M. Axelsson, L. Alakangas, An attempt to use LA-ICP-SMS to quantify enrichment of trace elements on pyrite surfaces in oxidizing mine tailings, J. Geochem. Explor. 92 (1) (2007) 1–12.
[11] J. Smuda, B. Dold, J.E. Spangenberg, H.R. Pfeifer, Geochemistry and stable isotope composition of fresh alkaline porphyry copper tailings: implications on sources and mobility of elements during transport and early stages of deposition, Chem. Geol. 256 (1–2) (2008) 62–76.
[12] P.M. Heikkinen, M.L Räisänen, R.H. Johnson, Geochemical characterization of seepage and drainage water quality from two sulphide mine tailings impoundments: acid mine drainage versus neutral mine drainage, Mine Water Environ. 28 (2008) 30–49.
[13] A. Parviainen, Tailings Mineralogy, Geochemistry at the abandoned Haveri Au–Cu Mine, SW Finland, Mine Water Environ. 28 (2009) 291–304.
[14] B. Dold, L. Fontboté, Element cycling and secondary mineralogy in porphyry copper tailings as a function of climate, primary mineralogy, and mineral processing, J. Geochem. Explor. 74 (1–3) (2001) 3–55.
[15] L. Alakangas, B. Öhlander, A. Lundberg, Estimation of temporal changes in oxidation rates of sulphides in copper mine tailings at Laver, Northern Sweden, Sci. Total Environ. 408 (2010) 1386–1392.
[16] J. Smuda, Geochemical evolution of active porphyry copper tailings impoundments: from alkaline deposition towards acidification, PhD thesis, University of Lausanne, 2009.
[17] M.G. Macklin, P.A. Brewer, D. Balteanu, T.J. Coulthard, B. Driga, A.J. Howard, S. Zaharia, The long term fate and environmental significance of contaminant metals released by the January and March 2000 mining tailings dam failures in Maramures County, upper Tisa Basin, Romania, Appl. Geochem. 18 (2003) 241–257.
[18] G. Bird, P.A. Brewer, M.G. Macklin, D. Balteanu, M. Serban, B. Driga, S. Zaharia, River system recovery following the Novat-Rosu tailings dam failure, Maramures County, Romania, Appl. Geochem. 23 (12) (2008) 3498–3518.
[19] J. Amezaga, A. Kroll, in: C. Wolkersdorfer, R. Bowell (Eds.), European Union Policies and Mine Water Management Contemporary reviews of mine water studies in Europe, Mine Water Environ. 24 (2005) 3–4.
[20] M. Grozea, The Certej failure 1971, the largest tailings dam accident in Romania, Hidrotehnica 41 (8) (1996) 23–28 (in Romanian).
[21] L. Grancea, M. Cuney, J.L. Leroy, Mineralized versus barren intrusions: a melt inclusion study in Romania's Gold Quadrilateral, Earth Planet. Sci. 333 (2001) 705–710.
[22] M. Borcos, S. Vlad, G. Udubasa, B. Gabudeanu, Qualitative and Quantitative Metallogenetic Analysis of the Ore Genetic Units in Romania, Geological Institute of Romania, Bucharest, 1998.
[23] F. Neubauer, A. Lips, K. Kouzmanov, J. Lexa, P. Ivascanu, 1: Subduction, slab detachment and mineralization: the Neogene in the Apuseni Mountains and Carpathians, Ore Geol. Rev. 27 (2005) 13–44.
[24] I.P.E.G. Hunedoara Deva, Documentation of Ore Calculation for Polymetallic and Gold–Silver Mineralization in the Hondol-Coranda, 1976 (in Romanian).
[25] B. Dold, Speciation of the most soluble phases in a sequential extraction procedure adapted for geochemical studies of copper sulphide mine waste, J. Geochem. Explor. 80 (2003) 55–68.
[26] D.L. Parkhurst, C.A.J. Appelo, User's guide to PHREEQC (Version 2)—A Computer Program for Speciation, Batchreaction, One-Dimensional Transport, and Inverse Geochemical Calculations, U.S. Geological Survey, Denver, 1999.
[27] J.W. Ball, D.K. Nordstrom, User's Manual for WATEQ4F, with Revised Thermodynamic Database and Test Cases for Calculation Speciation of Major, Trace, and Redox Elements in Natural Waters, 1991.
[28] B. Dold, Basic concepts in environmental geochemistry of sulfide mine-waste management, in: S. Kumar (Ed.), Waste Management, InTech Open Access Publications, 2010, pp. 173–198, http://www.intechopen.com/books/show/title/waste-management.
[29] U. Schwertmann, J. Friedl, H. Stanjek, From Fe(III) ions to ferrihydrite and then to hematite, J. Colloid Interface Sci. 209 (1999) 215–223.
[30] B. Dold, D.W. Blowes, R. Dickhout, J.E. Spangenberg, H.R. Pfeifer, Low molecular weight carboxylic acids in oxidizing sulfide mine tailings, Environ. Sci. Technol. 39 (2005) 2515–2521.